Tunable two dimensional optical beam steering with reconfigurable indium tin oxide plasmonic reflectarray metasurface

2016 J. Opt. 18 125003

(http://iopscience.iop.org/2040-8986/18/12/125003)

IOP Publishing Journal of Optics
J. Opt. 18 (2016) 125003 (6pp) doi:10.1088/2040-8978/18/12/125003

Tunable two dimensional optical beam steering with reconfigurable indium tin oxide plasmonic reflectarray metasurface

A Forouzmand and H Mosallaei

Computational EM and Physics Laboratory, Electrical and Computer Engineering Department, Northeastern University, Boston, Massachusetts 02115, USA

E-mail: Hosseinm@ece.neu.edu

Received 1 July 2016, revised 7 September 2016
Accepted for publication 20 September 2016
Published 1 November 2016

Abstract

In this paper, an electrically tunable reflectarray metasurface for two dimensional (2D) beam steering is designed by integration of a thin layer of indium tin oxide (ITO) material into a metal-insulator-metal (MIM) plasmonic unit-cell. The reflectarray is composed of square-shaped patch nanoantennas placed on a stack of insulator-ITO-metallic ground plane. The resonant characteristic of unit-cell and the accumulation of carrier density at the interface of ITO-insulator play key roles in obtaining over 250° of phase agility at around 218 terahertz (THz), by electrically varying the bias voltage. An array of unit-cells with integrated ITO and 2D voltage biasing distribution (from the side) offer the possibility of designing a reconfigurable antenna in which the main beam can be steered to relatively large angles in both θ- and φ- planes at carefully selected operating frequency. The significant advantage of this design is the dynamically adjustable radiation pattern in both azimuth and elevation planes even after fabrication.

Keywords: metasurfaces, optical engineering, phase shift, beam steering, indium tin oxide

(Some figures may appear in colour only in the online journal)

1. Introduction

In general, a reflectarray antenna includes an array of reflecting elements with the capability of controlling the reflection phase (ideally 360°) for each element which will lead to the creation of a desired wavefront. This phase variation has been realized commonly through utilizing elements having variable geometry, physical dimensions, and orientation [1, 2]. Since the functionality of the conventional reflectarray antennas is restricted to a fixed beam profile and cannot be tuned after fabrication, the modeling and design of an electrically tunable metasurface has significant importance. In microwave regimes, electrically tunable reflectarrays have been implemented by integrating varactor and PIN diodes within the inclusions [3–5]. By tuning the reversed applied voltage the varactor's capacitance and the operating states of PIN diodes can be changed which result in the control of the reflection phase. The recent advances in gate-tunable materials could facilitate the realization of reconfigurable metasurfaces in broad ranges of THz to near infrared (NIR) spectrums. In low-THz frequencies, graphene has versatile tunability by the change of electrochemical potential via chemical doping, magnetic field, and electrostatic gating. In [6], a tunable graphene-based reflectarray antenna has been proposed in which the phase of the reflected field at each square graphene patch as a building block of the proposed array can be controlled through the chemical potential variation and adjustment of the surface conductivity of graphene.

As a promising candidate in the NIR regime, the integration of transparent conducting oxide materials like ITO into a metasurface under the influence of an applied external voltage can lead to a significant advantage of adjustable functionality. The presented ITO applications can be divided into two main categories. First, metal-oxide-semiconductor (MOS) multilayer stack is deposited on top of a silicon waveguide [7–10]. The physical mechanism behind these

plasmonic modulators is the control of gap plasmonic modes through the ITO accumulation layer. An ultracompact 'PlasMOStor' consisting of an ITO-filled slot plasmonic waveguide which operates based on field-effect modulation has been studied in [11–15]. Second, an ITO-insulator layer is embedded in metal from both sides [16]. The light can be strongly confined in MIM structures due to its Fabry-Pérot-like resonance [17]. This well-known feature can be utilized to achieve total absorption or facilitate the manipulation of light. A perfect electrically tunable infrared absorption is realized by a thin layer of ITO deposited on an array of gold nanostrip antennas in [18].

In [19], it has been demonstrated that integration of ITO into strip antennas can steer the beam towards a desired diffracted angle in the θ- plane (one dimensional beam scanning) by applying different voltages to multi-level grating systems. This reflectarray antenna can operate only over the electric field with polarization perpendicular to the vertical strips. Following this idea, we leverage the resonant property of MIM structures and the gate-tunability of ITO to realize an electrically tunable reflectarray capable of two dimensional (2D) beam steering (both θ- and φ- planes) and operating over both linear polarizations (i.e. perpendicular and parallel) at NIR regime. The integration of a thin layer of ITO into a square-shaped patch nanoantenna as the building block of plasmonic reflectarray offers the feasible control over the phase of each element via the tunable gate biasing of ITO. We employ the phased array concept which is based on the individual biasing and managing the progressive phase-delay of nanoantennas in an array to manage the beam steering angle. The unit-cells are linked by connecting wires inserted in between thus the DC voltages can be simply applied from one side of the structure.

2. Design and structural parameters

Figure 1(a) demonstrates the schematic overview of the proposed electrically tunable reflectarray antenna. A square-shaped patch antenna is considered with the width of $w = 320$ nm and the period of $P = 500$ nm. The stand-off layer consists of a 26 nm-thick ITO layer and a 12 nm-thick alumina ($\varepsilon_{Al_2O_3} \approx 3$) which is placed between an optically thick gold substrate (back mirror) and an upper gold patch. The thickness of the back mirror substrate is chosen to be larger than skin depth of gold and its value is fixed at 100 nm. The optical behavior of gold is described through its dispersive permittivity which can be approximated by the Drude model in the NIR spectral region as: $\varepsilon_{Au}(\omega) = \varepsilon_0[\varepsilon_\infty - \omega_p^2(\omega(\omega + i\Gamma))^{-1}]$, with $\varepsilon_\infty = 1.53$, the plasma frequency of $\omega_p = 2\pi \times 2.069$ PHz, and the collision frequency of $\Gamma = 2\pi \times 17.64$ THz. The proposed 1D and 2D voltage biasing structures are also shown in figures 1(b) and (c), respectively. The DC voltage is applied across the top gold nanopatch and the bottom gold back mirror. It will be shown that the thin biasing lines which are inserted in-between have negligible artifacts on the element response. In figure 1(b), all elements located in the same row are

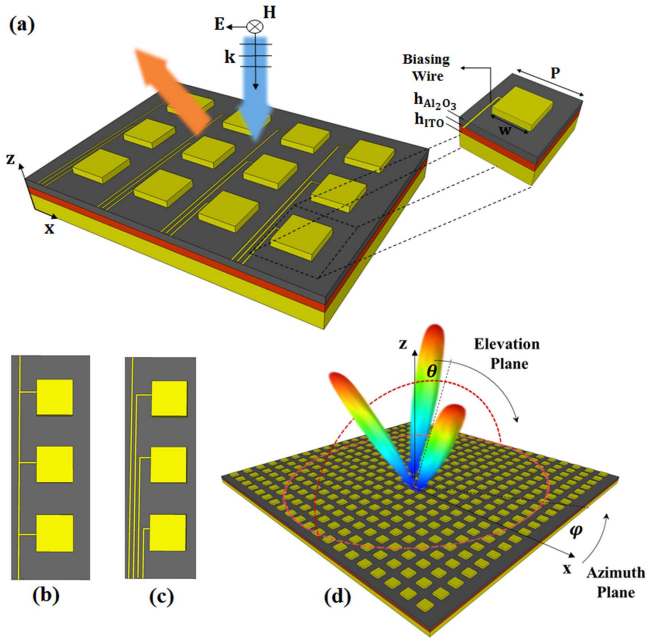

Figure 1. (a) Schematic representation of the proposed reflectarray metasurface for electrically tunable beam steering. (b) 1D and (c) 2D biasing schemes in order to achieve dynamic phase control over the unit-cells. (d) General concept of realizing an adjustable radiation pattern to any spatial 2D direction [θ, φ].

electrically net connected and will be managed by the same bias voltage and the different rows can be independently biased. Therefore, a 1D beam scanning (elevation plane) can be achieved. Figure 1(c) shows another biasing layout which can be utilized to obtain more degrees of freedom and control each unit-cell individually, thus the radiation pattern can be manipulated in both elevation and azimuth planes as shown schematically in figure 1(d).

The general properties of the ITO film are attributed to both pre- and post-deposition treatments as well as the used technique. Sputtering is the most well-known approach in comparison with other methods such as spray pyrolysis and screen printing for the deposition of ITO. By controlling the ITO sputtering process via the oxygen content, the tin-to-indium ratio, temperature, and pressure, various values of dielectric function of ITO are reported in [7–16, 18–20]. The permittivity of conducting oxide ITO can be described by a Drude function in which ω_p, ε_∞, and Γ are usually calculated by data fitting of the experimentally obtained transmittance and reflectance of the ITO film. Plasma frequency is related to the carrier density N and the electron effective mass $m^* = 0.35 \times m_0$ as $\omega_p^2 = Ne^2/(\varepsilon_0 m^*)$, where e is the electron charge and m_0 is the electron rest mass. In order to shift the plasma frequency into the NIR regime, the carrier concentration should be in the range of $10^{20} - 10^{21}$ cm^{-3}. In this paper, it is assumed that the background carrier concentration of ITO is 3×10^{20} cm^{-3}($\omega_p = 1.6517 \times 10^{15}$ rad s^{-1}), $\varepsilon_\infty = 2.17$, and $\Gamma = 190$ THz [18, 19].

In [9, 16], the effect of the applied voltage bias on the carrier density of the ITO layer is studied based on the Thomas–Fermi screening theory and the averaging of the carrier density over the whole ITO layer. In a more accurate

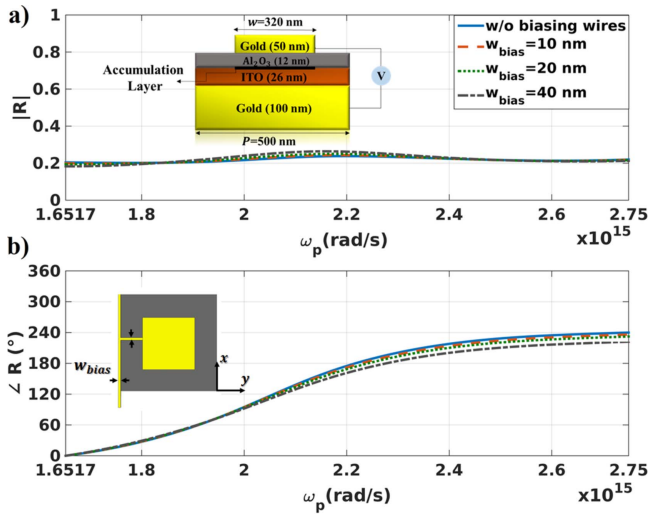

Figure 2. (a) Amplitude and (b) phase of the reflection coefficient as a function of the effective plasma frequency of the accumulation layer at the operating frequency of $f = 218.2$ THz. The reflection response is studied for different widths of connecting wires ($w_{\text{bias}} = 10$, 20, and 40 nm) and negligibly perturbed. The insets of (a) and (b) show the cross-sectional and top views of unit-cell with the structural parameters, respectively.

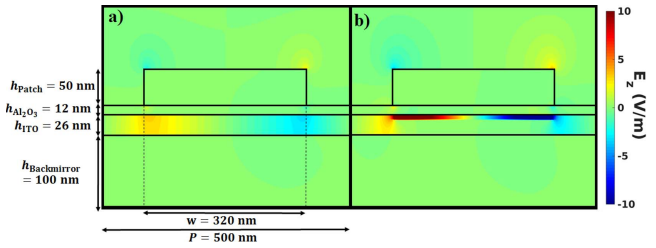

Figure 3. The near field distribution of the normal component of electric field (E_z) in the x–z plane (a) without the gate bias and (b) with sufficient gate bias to form near-zero permittivity ($\omega_p = 2.0 \times 10^{15}$ rad s^{-1}) at the active layer of ITO (Al_2O_3-ITO interface).

approach, an ultra-thin accumulation layer (5 ± 1 nm) can be considered at the insulator-ITO interface in which the refractive index alters with the applied field [20]. Under the applied modulating voltage (0 V to 2.5 V), the carrier concentrations at the insulator-ITO interface increases (1×10^{21} to 2.83×10^{22} cm^{-3}). This change in the carrier density is accompanied by the increment of the effective plasma frequency (2.097×10^{15} to 4.672×10^{15} rad s^{-1}) and unity-order refractive index changes within an ultrathin (5 ± 1 nm) accumulation layer (table 1 in [20]). In this paper, we follow the latter approach and a 0.66-fold increase of plasma frequency of ITO (1.6517×10^{15} to 2.75×10^{15} rad s^{-1}) is considered which is attainable based on the presented experimental results in [19, 20]. In [19], a 5-fold increase of the carrier concentration (i.e. 1.45-fold increase of the plasma frequency) has been achieved by varying the voltage bias from 0 to 6 V. It is worth noting that the breakdown voltages for various thicknesses of the Al_2O_3 insulation layer (2 nm, 5 nm, and 10 nm) have been determined in the supporting information of [14]. Here, a 12 nm-thick alumina is assumed to guarantee a breakdown voltage higher than 4 V.

Figures 2(a) and (b) represent the finite-difference time-domain (FDTD) full-wave simulation results for the realized reflection amplitude and phase of the proposed unit-cell excited by x-polarized incident wave for different plasma frequencies of the accumulation layer at the operating frequency of 218.2 THz. The reflection amplitude is almost constant and varies slightly around 0.2. This is also consistent with the results presented in [19]. In addition, a wide range of phase changes (≈250°) is realized through the coincidence of two physical phenomena. First, the patch unit-cell behaves as a Fabry–Pérot-like resonator for the guided modes in the insulator layer at $f = 218.2$ THz. This resonance is a well-known characteristic of MIM structures and it has been widely utilized in fixed beam reflectarray antennas to achieve desired phase distributions by changing the period, height, and width of gold nanopatches. Second, by the increment of the voltage bias between the gold nanopatch and the back mirror, the carrier density in ITO increases and an accumulation layer will be formed at the Al_2O_3-ITO interface (black line in the inset of figure 2(a)). This results in the variation of the effective plasma frequency (corresponding to the complex permittivity) and a change in the phase of the reflected beam. Specifically, the physical mechanism behind this phenomenon can be described as the significant phase change which occurs due to the zero-crossing of permittivity of the active layer of ITO. The effect of biasing lines on the performance of unit-cells are also studied. As shown in figure 2, the reflection response is negligibly disturbed for different widths of biasing lines ($w_{\text{bias}} = 10$, 20, and 40 nm). The thickness of biasing lines is considered ≈5 nm (skin depth of gold in the operating frequency). It is a well-known concept in microwave regimes that when the width of connecting wires is very thin, the wire grid will not affect much the antenna radiation [21, 22]. It may only cause an insignificant cross polarization. In addition, the radiation of a biasing line as a horizontal current element (parallel to x-y plane) will be cancelled based on the image theory in the presence of a ground plane. It is worth noting that the patch antenna has a magnetic mode radiation mechanism [23].

When the unit-cell is not biased, the background and active layer of ITO have the same positive dielectric constants ($0 < \varepsilon_{\text{ITO}} < 1$) thus acts like a dielectric. Figure 3(a) represents the near field distribution of the normal component of the electric field (E_z) which clarifies the dielectric characteristic ($\varepsilon_{\text{ITO}} = 0.745 + 0.198i$) of the ITO layer without any significant electric confinement in the active layer of ITO. With a gate voltage, the 26 nm-thick ITO layer splits into two layers, a 20 nm unaffected layer and a 6 nm accumulation layer. By the increment of the voltage bias, the permittivity of active ITO decreases and phase change becomes more significant. Figure 3(b) clearly represents a considerable electric field confinement at Al_2O_3-ITO interface with near-zero permittivity ($\varepsilon_{\text{ITO}} = 0.08 + 0.2897i$). At the interface of ITO and Al_2O_3, the normal components of the electric flux density should be continuous. Therefore, an intensive electric field will be excited at the boundary once the permittivity of ITO goes to zero.

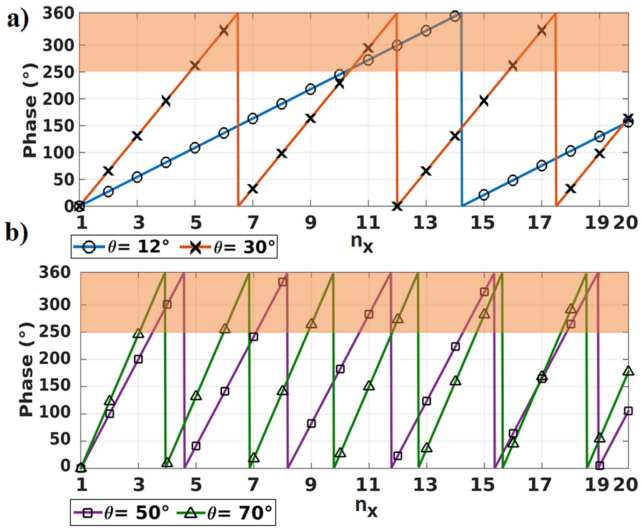

Figure 4. (a)–(b) The required phase discontinuity to steer the impinging plane wave towards $\theta = 12°$, 30°, 50°, and 70° at $f = 218.2$ THz. The markers indicate the sampling of the phase profile at each unit-cell.

3. One-dimensional beam steering

In order to design a reflectarray with the possibility of reflecting the x-polarized incoming beam into a specific direction of θ (angle from the z-axis) and φ (angle from the x-axis) as shown in figure 1(d), the required reflection phase-delay distribution in the x–y plane can be calculated based on the phased array concept as $\psi(x, y) = (2\pi/\lambda)\sin\theta(x\cos\varphi + y\sin\varphi)$ [1]. As a starting point, we assume a 20 × 20 ($7.25\lambda \times 7.25\lambda$) array of plasmonic patch antennas with a 1D biasing scheme in such a way that the elements which are in the y-direction have the same voltage bias. In other words, the reflectarray is uniform along the y-direction resulting in $\varphi = 0$ (elevation plane). In order to realize a reflection with the steering angles of $\theta = 12°$, 30°, 50°, and 70° at $f = 218.2$ THz, the required phase profiles, $\psi(x)$, are plotted in figures 4(a) and (b). In our approach, the continuous phase function is approximated with discrete steps (markers in figure 4) in the x-direction and the unit-cells along the y-axis are kept with the same phase shift. In figure 4, n_x refers to the unit-cell number along the x-direction. It is worth noting that a unit-cell cannot cover phase delays larger than 250° (as shown in figure 2(b)) so the required phase shifts larger than this limitation (the shadow regions in figures 4(a) and (b)) are just replaced by the maximum possible phase change (250°). In other words, those elements are assumed under the influence of maximum possible voltage bias ($\omega_p = 2.75 \times 10^{15}$ rad s^{-1}). It will be shown that this approximation has negligible effects on reflectarray antenna performance.

Figures 5(a)–(d) show the full-wave FDTD simulation results for the 2D normalized intensity of the reflected beams back into $\varphi = 0°$ and $\theta = 12°$, 30°, 50°, and 66.5°. As shown in figure 5(e), the half power beam width (HPBW) of reflected beams are achieved, 7.5°, 8°, 10.5°, and 16.5°, in the x–z plane. It can be clearly seen that the designed metasurface scans the beam in the desired direction, but as

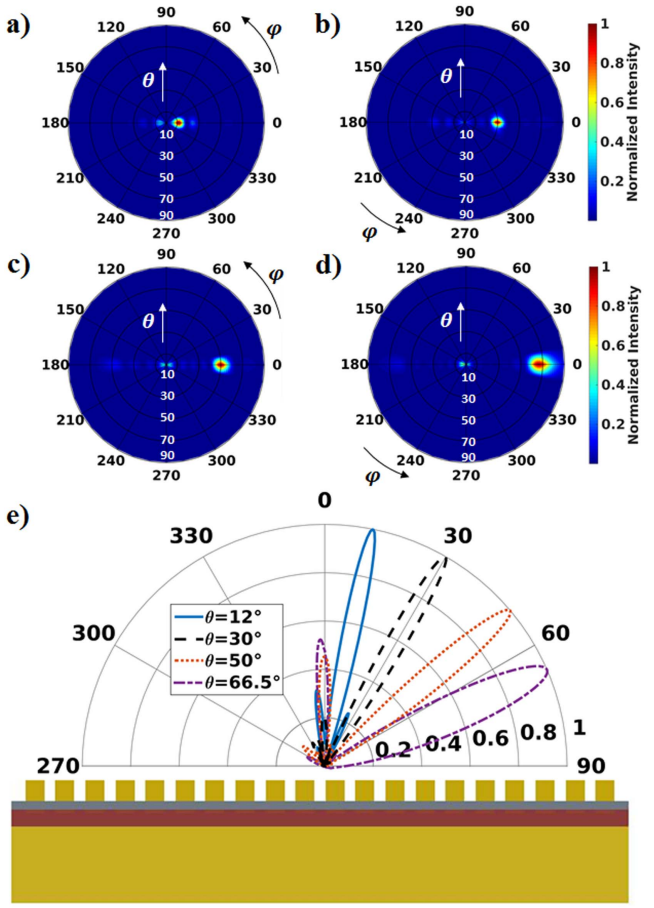

Figure 5. (a)–(d) Full-wave FDTD simulation results for the 2D normalized intensity of the reflected beam in $\varphi = 0$ and $\theta = 12°$, 30°, 50°, and 66.5° for the x-polarized incident beam. (e) The results in (a)–(d) in the x–z plane (elevation plane).

expected, the increment of the steering beam angle would result in some destructive effects such as larger side lobes, the fat profile of the main lobe, and a shift of the intensity peak position. These artifacts arise due to the finite size of the array, the imperfect realization of the required phase, and abrupt phase change in neighbour elements. Fortunately, the level of the sidelobes and the shift of maxima are not significant enough to cause a considerable effect on the performance of the reflectarray antenna. In this section, we restrict our design to finite 20 × 20 array and the entire array is modelled and investigated accurately by FDTD simulation in order to consider all in-plane coupling effects between elements. A larger array can ameliorate the previously mentioned artifacts because of two key reasons. Firstly, based on the antenna theory and phased array concept [23], increasing the overall length of a reflectarray antenna (aperture size) can help to concentrate the light with a narrower divergence angle (smaller HPBW) and also to reduce the side lobes. Secondly, the unit cells of the antenna array are oriented in an aperiodic scheme to realize the required phase distribution. It should be mentioned that although the elements are geometrically the same, the active layers of ITO below nanoantennas become different according to different applied voltages. When the reflectarray becomes larger, each unit-cell behaves much

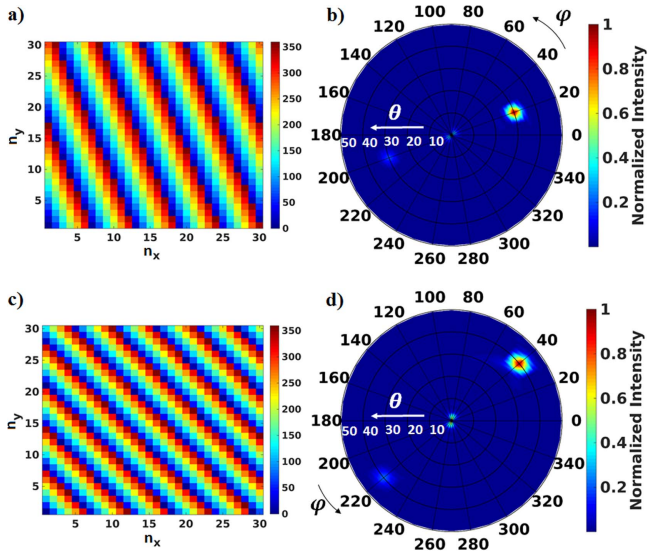

Figure 6. The required phase distributions for the nanopatch antennas and the 2D normalized intensity to scan the beam with (a)–(b) $[\theta, \varphi] = [30^\circ, 20^\circ]$ and (c)–(d) $[\theta, \varphi] = [40^\circ, 40^\circ]$.

closer to periodic characteristics (figure 2). The required phase distribution to steer a y-polarized beam towards a desired angle of $[\theta, \varphi]$ can be calculated in a similar fashion and due to the symmetrical geometry of unit-cell along both x and y directions, the results of figure 2 can be utilized in order to calculate the required effective plasma frequency at the accumulation layer (associated with the required DC voltage bias) to realize the phase delay at each unit-cell. The beam scanning results for y-polarized beams are omitted here for the sake of brevity.

4. Two-dimensional beam steering

In the 1D reflectarray antenna design, the phase distribution varies only in the x-direction (or y-direction). As a consequence, it can only manipulate the incident beam in the x–z (or y–z) plane. This implicitly means that the optical device is unable to steer the beam toward all the desired points in the space. This crucial restriction reveals the necessity of designing a reflectarray antenna with the capability of 2D beam scanning. To realize this metasurface, both phase distributions for x and y directions should be satisfied which dictate applying a 2D biasing layout as shown in figure 1(c). The required interfacial phase distribution to steer the incident beam at $\varphi = 20^\circ$ and $\theta = 30^\circ$ for a 30×30 array ($\approx 11\lambda \times 11\lambda$) metasurface is plotted in figure 6(a). Therefore, we must find the proper effective plasma frequency at the accumulation layer of each unit-cell (figure 2(b)) in order to consider the effect of the required DC voltage bias in our simulation. The 2D normalized intensity of the steered beam is shown in figure 6(b) which is in a great agreement with the desired direction calculated from the phased-array theory [1]. In order to provide more clarification regarding the performance of the presented metasurface, we redesign the array to steer the light in large scanning angles of $\theta = 40^\circ$ and $\varphi = 40$. Fortunately, the array is sufficiently large to successfully demonstrate the beam scanning capability of the antenna even for such great angles in both θ and φ simultaneously [figures 6(c) and (d)]. In figures 6(a) and (c), n_x and n_y refer to the unit-cell numbers along x- and y-directions.

5. Conclusions

In summary, an electrically tunable reflectarray plasmonic patch nanoantennas with potential for 1D and 2D beam steering in the NIR regime is designed by integrating a thin layer of ITO into the patch substrate. The scanning angle can be feasibly controlled by adjusting the 1D/2D voltage biasing distribution, and feed network from the side. To the best of our knowledge, this is the first time that 2D beam scanning by ITO-plasmonic patch antennas is demonstrated. The presented methodology is of significant interest and can be realized at any NIR operating frequency with controlling the parameters of ITO films along the deposition technique.

Acknowledgments

This work is supported in part by the U.S. Air Force Office of Scientific Research (AFOSR), #FA9550-14-1-0349 and in part by Defense Advanced Research Projects Agency (DARPA) award via Grant # N00014-14-1-0850. The authors would like to appreciate the generous computing resources provided by the Northeastern University Discovery Cluster. The authors are also grateful to the reviewers for their valuable comments.

References

[1] Farmahini-Farahani M and Mosallaei H 2013 *Opt. Lett.* **38** 462–4
[2] Ahmadi A, Ghadarghadr S and Mosallaei H 2010 *Opt. Express* **18** 123–33
[3] Boccia L, Venneri F, Amendola G and Massa G D 2002 Application of varactor diodes for reflectarray phase control *Antennas and Propag. Soc. Int. Symp. (San Antonio, TX, 2002) IEEE* pp 132–5
[4] Boccia L, Amendola G and Massa G D 2004 A microstrip patch antenna oscillator for reflectarray applications *Antennas and Propag. Soc. Int. Symp.* vol 4 *IEEE* pp 3927–30
[5] Sievenpiper D F, Schaffner J H, Song H J, Loo R Y and Tangonan G 2003 *IEEE Trans. Antennas Propag.* **51** 2713
[6] Carrasco E, Tamagnone M and Perruisseau-Carrier J 2013 *Appl. Phys. Lett.* **102** 104103
[7] Tabei T and Yokoyama S 2012 *Proc. SPIE* **8431** 84311K
[8] Lu Z, Zhao W and Shi K 2012 *IEEE Photo. J.* **4** 735–40
[9] Melikyan A *et al* 2011 *Opt. Express* **19** 8855
[10] Sorger V, Lanzillotti-Kimura N, Ma R and Zhang X 2012 *Nanophotonics* **1** 17–22
[11] Dionne J A, Diest K, Sweatlock L A and Atwater H A 2009 *Nano Lett.* **9** 897–902
[12] Babiecheva V E and Laverinenko A V 2012 *Proc.SPIE* **8424** 842413
[13] Babiecheva V E, Kinsey N, Naik G V, Ferrera M, Laverinenko A V, Shalaev V M and Boltasseva A 2013 *Opt. Express* **21** 27326–37

[14] Lee H, Papadakis G, Burgos S, Chander K, Kriesch A, Pala R, Peschel U and Atwater H 2014 *Nano Lett.* **14** 6463–8
[15] Lu Z, Zhao W and Shi K 2014 (arXiv:1205.0502v1)
[16] Babicheva V and Lavrinenko A 2012 *Optics Commun.* **285** 5500–7
[17] Koechlin C, Bouchon P, Pardo F, Pelouard J L and Haïdar R 2013 *Opt. Express* **21** 7025–32
[18] Yi F, Shim E, Zhu A, Zhu H, Reed J and Cubukcu E 2013 *Appl. Phys. Lett.* **102** 221102
[19] Huang Y W, Lee H W, Sokhoyan R, Pala R, Thyagarajan K, Han S, Tsai D P and Atwater H A 2015 (arXiv:1511.09380)
[20] Feigenbaum E, Diest K and Atwater H 2010 *Nano Lett.* **10** 2111–6
[21] Ma X, Pan W, Huang C, Pu M, Wang Y, Zhao B, Cui J, Wang C and Luo X 2014 *Adv. Opt. Mater.* **2** 945
[22] Xu H X, Sun S, Tang S, Ma S, He Q, Wang G M, Cai T, Li H P and Zhou L 2016 *Sci. Rep.* **6** 27503
[23] Stutzman W L and Thiele G A 2012 *Antenna Theory and Design* (New York: Wiley)